J Mater Sci (2008) 43:1205–1213
DOI 10.1007/s10853-007-2277-3

Preparation of Semi-aromatic polyamide(PA)/multi-wall carbon nanotube (MWCNT) composites and its dynamic mechanical properties

Rui Song · Debin Yang · Linghao He

Received: 26 April 2007 / Accepted: 30 October 2007 / Published online: 12 December 2007
© Springer Science+Business Media, LLC 2007

Abstract Well dispersed semi-aromatic polyamide(PA)/multi-wall carbon nanotube (MWCNT) composite was prepared through high-speed shearing method in the presence of surfactant sodium dodecylbenzene sulfonate (SDBS). Further analysis of morphology, crystallization, and dynamical mechanical properties shows the presence of SDBS helps to disperse the MWCNT and largely enhance the mechanical property. In comparison with neat PA component, the storage modulus (E') of the blend system at 90 °C is 3.5 times larger than PA with MWCNT load ratio of 3 wt.%; and meanwhile the glass transition temperature (T_g) of PA component increases about 17 °C; Similar phenomena have not found in MWCNT/PA composite without surfactant. Simultaneously, as DSC and morphology measurements indicate, the filled MWCNT does not show tremendous effect on the crystalline phase and crystallinity of PA, which imply that the increasing mechanical property for composites is due to the strengthening effect of MWCNT itself, not being caused by the change of crystalline phase and crystallinity by the addition of MWCNT. The increasing T_g, indicative of the restricting movement of PA chains, is most probably ascribe to the strong interaction presented between MWCNT and PA chains.

R. Song (✉) · D. Yang · L. He
College of Materials and Chemical Engineering, Zhengzhou University of Light Industry, Zhengzhou 450003, China
e-mail: rsong@gucas.ac.cn

R. Song
College of Chemistry and Chemical Engineering, Graduate University of Chinese Academy of Sciences, Beijing 100039, China

D. Yang
e-mail: yangdebin2004@mail.china.com

L. He
e-mail: lhhe@zzuli.edu.cn

Introduction

The carbon nanotube as its unique tube-like structure and very high aspect ratio which directly measured by transmission electron microscopy [1], results in its extraordinary mechanical properties (strength and flexibility), making them ideal reinforcing material, especially in the region of carbon nanotube reinforcing polymer region, which have been investigated for flame-retardant performances [2], improved electrical conductivity and electrostatic charging behavior [3, 4], and in lightweight, high strength composites [5]. However, fabrication of homogenous nanocomposites with carbon nanotube, which determines the final property of carbon nanotube filled material, remains a technical challenge [6]. Up-to-date, surface modification [5], high-power sonication [7], and surfactant assistant dispersion [8] were among the usually used methods to disperse carbon nanotube into polymer matrix. Liu et al. [5] added the water-soluble single wall carbon nanotube (SWCNT) with surface bonding hydroxyl (S–OH) groups into poly(vinyl alcohol)(PVA), obtaining an increase of 47% in the tensile yield strength and a glass transition temperature (T_g) increased from 68.8 °C to 74.3 °C for PVA/0.8 wt.% S–OH. Ruan et al. prepared the multi-wall carbon nanotube (MWCNT)-ultrahigh molecular weight polyethylene successfully using the ultrasonic vibration, reached to a 25% increase in Young's modulus and 47.6% increase in yielding stress at the addition content of 1 wt.% [9]. Similarly, employing the high-power

sonication step, Chang et al. incorporated the SWNT into polypropylene matrix with sharp increased tensile modulus (E) of the fibers with addition of 1 wt.% SWCNT; however, E values increased much slower with further addition of SWCNT; while the tensile stiffness increased only ~45% when the concentration of SWCNT increases from 1 wt.% to 4–5 wt.% [7]. Through surfactant-assisted processing of carbon nanotube, Gong et al. obtained the epoxy-CNT composite and its storage modulus was increased by more than 30%, and T_g temperature was elevated from 63 °C to 88 °C as compared with the pure epoxy sample; on the other hand, addition of carbon nanotube only gave a moderate increase in storage modulus and T_g [8].

It seems that what methods should be adopted to disperse the carbon nanotube was highly depend on the property of its host polymer. In this investigation, semi-aromatic polyamide (PA) chains containing benzene rings with the π-electron-cloud structure would generate π–π stack interaction with the surface of carbon nanotube, which is known to have a large π-electron-cloud structure. Therefore, we proposed that the strong interactions originally exist in between benzene ring and carbon nanotube. To this end, the MWCNT was added into PA matrix via. high-speed shearing step in the presence of surfactant sodium dodecylbenzene sulfonate (SDBS). The resulting composites showed improving MWCNT dispersity and enhancing mechanical properties. In this case, the storage modulus of the composite (with load ratio of 3 wt.% MWCNT/PA-SDBS) at 90 °C increases 3.5 times larger than PA; while the T_g temperature for this sample increased ca. 17 °C in comparison to the virgin PA component without surfactant. All these observations imply the effective strengthening role of carbon nanotube to PA matrix.

Experimental

Sample preparation

Multi-wall carbon nanotubes were supplied from Shenzhen Nanotech Port Co. Ltd., with purity of 95 wt.%, diameter and length of ca. 50 nm and 15 ~ 20 μm, respectively (as shown in Fig. 1, obtained from JEM 100CX-II transmission electron microscope). PA—developed by using terephthalic acid, *m*-phthalic acid, and aliphatic diamines by means of polycopolycondensation—was supplied by Prof. J. Z. Chen of Zhengzhou University, China. The detail about this kind of polyamide could be found elsewhere [10].

The pristine MWCNTs were purified according to the literature method [11, 12] prior to use. Briefly, pristine MWCNTs were refluxed 24 h at 80 °C in concentrated nitric acid. The excess nitric acid was removed by centrifuging. The resulting black solid was washed thoroughly with deionized water until the pH value of the water was about 5 ~ 6. The purified MWCNT was then dried at 50 °C in a vacuum to remove water completely. This process, in addition to remove the impurity such as amorphous carbon and metal catalyst, is also able to bond carboxylic acid groups onto the surface of carbon nanotube and generate defects on the surface of carbon nanotube. This treatment, therefore, can increase the miscibility of carbon nanotube with polymer matrix, but make the mechanical properties of carbon nanotube deteriorated. In this experiment, the purifying process is only to exclude the impurity and the other effect is non-considered temporarily.

For preparation of MWCNT/PA, the purified MWCNTs were dispersed in a homogeneous 0.9 g L^{-1} sodium dodecylbenzene sulfonate (SDBS; i.e., $C_{18}H_{29}SO_3Na$)-methyl phenol solution via a high-speed shearing (11,000 rpm) step for 2 h with a 20-mL suspension volume to make the MWCNT homogeneously dispersed [13]. In this case, the content of SDBS to methyl phenol was fixed at 0.9 g L^{-1} for all samples for the sake of comparison; then, the PA solution (PA/methyl phenol = 10 wt.%) was entirely dissolved into the suspension at a magnetic stirring process at ambient temperature for 12 h to get the viscous suspension. The load ratios of MWCNT to PA are 0.1, 0.5, 1, and 3 wt.%, respectively. For comparison, the PA/methyl phenol and PA/SDBS/methyl phenol solution were also prepared according to the above method. To prepare the test film specimens the blend mixtures were cast onto the well-cleaned flat glass slide through a spin-coating process and were then put in a vacuum oven at 100 °C for 2 days to remove the excess methyl phenol.

Characterization

Sample morphologies were recorded using Nikon Eclipse E600 polarized optical microscope (POM). The photographs for the sample films were taken with a Nikon Coolpix 5,600 digital camera equipped on the vertical hood of the optical microscope.

For DSC test, all samples were analyzed by Q100 Temperature Modulated DSC from TA Corporation, which equipped with the thermal analysis data system for the corrections of scan baseline, transition temperature, and enthalpy value. With standard mode, the sample of 5 ± 0.2 mg was heated at a heating rate of 10 °C/min from ambient temperature to 250 °C, isothermalized for 1 min and then cooled down to ambient temperature at the same rate.

Surface analysis of membranes was done by atomic force microscopy (AFM) using a DI Nanoscope IIIA

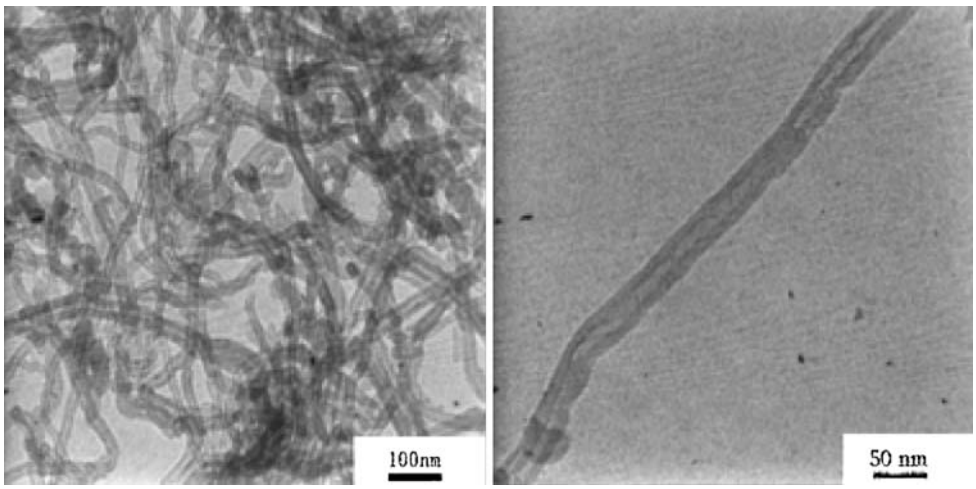

Fig. 1 TEM images of receiving original MWCNT, left: low magnification, right: high magnification

Multimode Scanning Probe Microscope (Digital Instruments, Veeco Metrology Group, Santa Barbara, CA, USA) at ambient conditions. Sample films were attached onto iron AFM substrate disks using double-sided tape. Topographic images were obtained in tapping mode using commercial silicon microcantilever probes (M1, Nanotools, Germany) with a tip radius of $\sim$10 nm and spring constant $\sim$42 N/m. The probe oscillation resonance frequency was *ca*.330 kHz and scan rate was 1 Hz.

Raman spectra were collected for all samples using LabRAM HR system 6,400. The excitation source was an argon laser with the wavelength of 514.5 nm and the spectra data were collected in the 180 degree back-scattering mode. The laser beam was 25% de-focused together with a 50x objective lens to produce a 20–30 mm diameter laser spot to minimize laser beam heating effects as well as to have a larger sampling volume. To minimize stress relaxation as well as heating effects, five scans were used for each spectrum collection.

Infrared spectra were obtained using a FT-IR spectrophotometer (Bruker, Tensor 27), at the resolution of 4 cm^{-1}, 32 scans, and with single attenuated total reflection (ATR) mode. In this mode, thick sample can be directly tested by collecting the reflection information of single infrared beam on the sample surface.

A X-ray diffractometer (D8, Bruker, Germany) was used to inspect the diffractograms of the blend membranes at 25 °C. The X-ray source was Ni-filtered Cu Kα radiation (30 kV and 30 mA). The dry membranes were mounted on aluminum frames and scanned at a speed of 0.5°/min from 5° to 40° (2θ).

Dynamic mechanic thermal analysis (DMTA) experiments were performed under film tension mode with a TA instruments Q800 DMTA device at a heating rate of 3 °C/min from 30 to 140 °C, 1 Hz frequency. The stress-strain curves were obtained at ambient temperature, with the amplitude range of 50 μm. The sample dimension is $30 \times 5 \times 0.1$ mm^3. Choosing the dynamic testing technique is because it only requires small samples and provides information on both the thermal and mechanical properties [8]. Thermogravimetric analysis (TGA) was performed on a STA 409PC, from Netzsch Corp, Germany. The sample was heated from ambient temperature to 600 °C at a heating rate of 10 °C/min under a constant flow of nitrogen gas.

Results and discussion

Dispersity of CNT

Optical microscope images provide direct evidence for evaluating the quality of the composites. Figure 2 shows images of 1 wt.% MWCNT/PA and 1 wt.% MWCNT/PA-SDBS films, respectively. At micrometer-scale resolution, a less aggregated 1 wt.% MWCNT/PA-SDBS composites film is observed (Fig. 2(b)). By contrast, a more aggregated 1 wt.% MWCNT/PA film is formed (Fig. 2(a)). Generally, CNTs are known to disperse well in certain solutions in the presence of surfactant [14]. However, CNTs may aggregate again during the composites-forming process [5, 15]. From Fig. 2, we conclude that composite films based on surfactant-assisted nanotubes exhibit better homogeneity compared to nanotubes without surfactant, which proves that the adding surfactant effectively prevent the agglomeration in the process of solvent evaporating. In the meantime, we found that the agglomeration of CNT during the composites-forming process is also related to the spin-coating film thickness in this experiment.

Israelachvili et al. [16] thought that the surfactant would interact with carbon nanotube through the hydrophobic segment; as a coupling agent, the surfactant may introduce a steric repulsive force between the carbon nanotubes, which overcomes the Van der Waals attractive force between the carbon nanotube surface, suppressing the

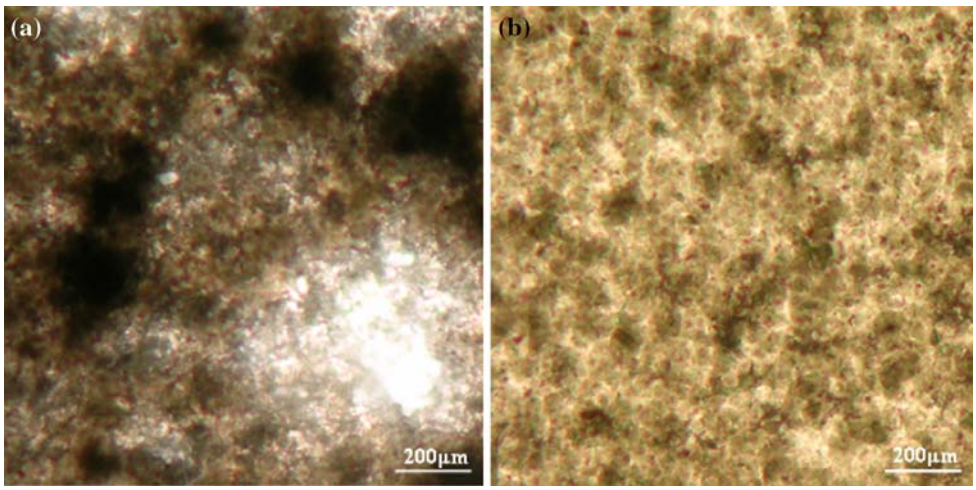

Fig. 2 Optical microscope images of composites, (**a**): 1 wt.% MWCNT/PA, (**b**): 1 wt.% MWCNT/PA-SDBS, SDBS/ methyl phenol = 0.9 gL^{-1}

agglomeration; and the hydrophilic segment can interact with the PA segment through hydrogen bonding, increasing the miscibility of CNT with polymer matrix.

Raman spectroscopy is a useful tool for the characterization of carbonaceous materials [17]. The typical G-band (derived from the graphite-like mode) is situated at 1,574 cm^{-1} in the spectrum of neat CNT (Fig. 3). In contrast to the graphite G-band, which exhibits a single Lorentzian peak, the band for CNT has a shoulder extending to higher wavenumbers. Disorder-induced D-band is situated at 1,326 cm^{-1} and its second-order harmonic D′-band is found at 2,660 cm^{-1}. From the D′-band in Raman spectra of MWCNT and its composites (see Fig. 4), before and after purification, there is not change occurred for the position of D′-band of CNT, indicating the purifying process has not damaged the structure of CNT severely. Interestingly, The D′-band of 1 wt.% CNT/PA has a large shift toward higher wavenumber and at the same content, this shift is retarded after the surfactant added, which was presumably ascribed to the coating of surfactant to CNT that covering the surface defect of CNT. After the coating of CNT with PA, the spectrum of this polymer dominates in all samples. We have observed the relative decrease and a shift up for the second-order of the disorder-induced D′-band and D band which indicates a less perfect structure for the nanotubes embedded in the polymer [18].

In some cases, Raman spectroscopy showed indications of possible interaction between single-wall CNT and conducting polymers [19]. In contrast to polymer-functionalized CNT, where strong effects of the polymer on the Raman signal of CNT have been observed [20, 21],

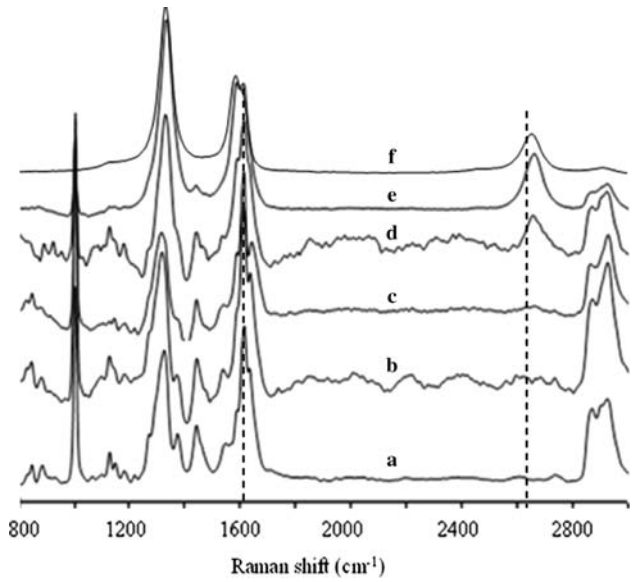

Fig. 3 Raman spectra of MWCNT, and its PA composites, (**a**): neat PA, (**b**): 0.1 wt.%, (**c**): 0.5 wt.%, (**d**): 1 wt.%, (**e**): 3 wt.%, (**f**): purified MWCNT

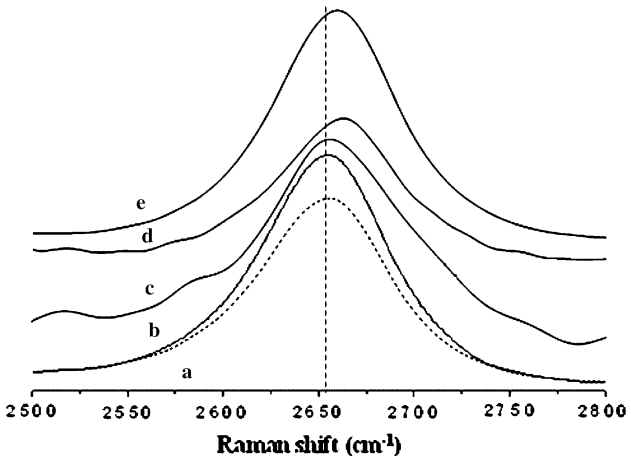

Fig. 4 D′-band Raman spectra of MWCNT, and its PA composites. (**a**): raw MWCNT, (**b**): purified MWCNT, (**c**): 1 wt.% CNT/PA-SDBS, (**d**): 1 wt.% CNT/PA, (**e**): 3 wt.% CNT/PA-SDBS

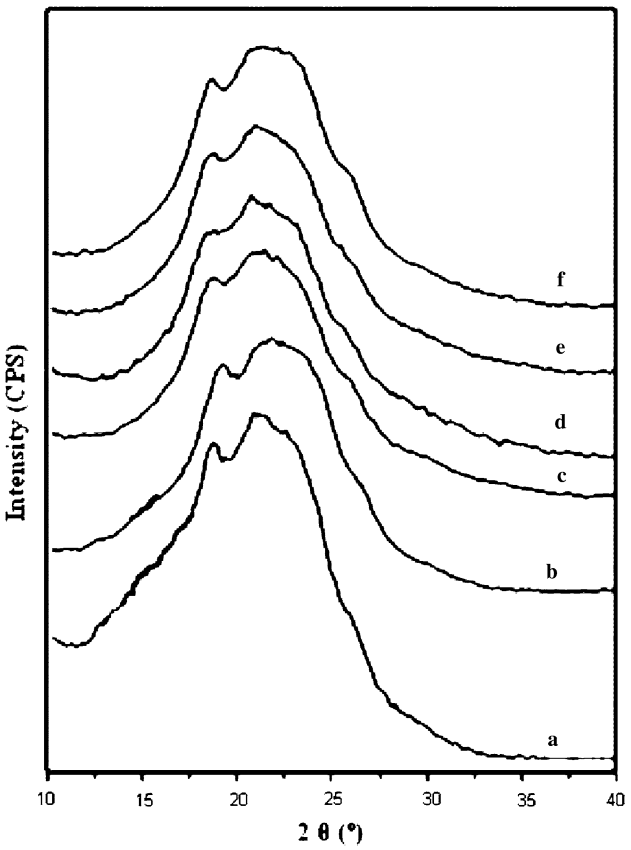

Fig. 5 XRD patterns of samples. (**a**): neat PA, (**b**): PA-SDBS, (**c**): 0.1 wt.% MWCNT/PA-SDBS, (**d**): 0.5 wt.% MWCNT/PA-SDBS, (**e**): 1 wt.% MWCNT/PA-SDBS, (**f**): 3 wt.% MWCNT/PA-SDBS

strong interaction between CNT and PA has been proved by Raman spectra in the present study.

Crystalline phase

Figure 5 represents the XRD patterns of MWNT/PA composites with different MWNTs contents (0, 0.1, 0.5, 1, and 3 wt.%). Only two peaks were observed at about $2\theta = 20°$ and 22° (assigned to the α-crystal) for the MWNT-reinforced composites [22]. This observation is consistent with our corresponding FT-IR results (not present) in which only typical α-characteristic absorbance occurred at *ca.* 1,477, 1,420, 1,201 cm^{-1} [23–25]. From the XRD and FT-IR data we could conclude that crystalline phase of PA was not changed by the addition of MWCNT and SDBS.

On the other hand, DSC measurements were performed for all samples to get the information of heat of fusion and T_g variation. In the typical DSC curves in Fig. 6, it could be readily noted that a wide endothermal process but no obvious melting peak is present with elevating temperature, which is an indication of poor sample crystallization. In

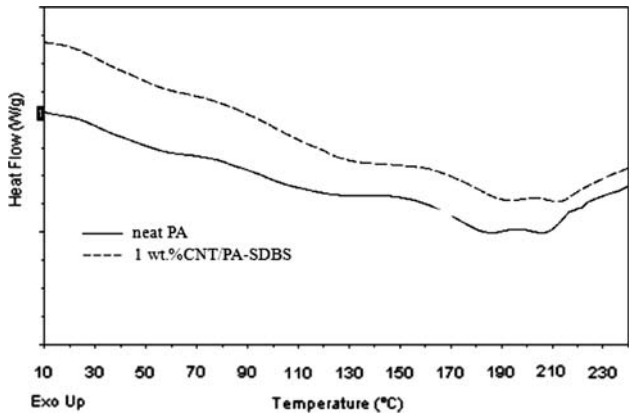

Fig. 6 Typical DSC curves of samples

order to quantify the crystallization degree, the areas of the endothermal stage at a defined temperature range is calculated as the heat of fusion of samples to quantitatively compare the crystallinity difference of the samples and the results are listed in Table 1. The calculating results indicate that the samples have similar, lower heat of fusion (Table 1), namely, they have similar crystalline degree. In addition, well-resolved glass transition could not be detected from the DSC curves due to the wide endothermal peak.

The typical AFM images in Fig. 7 reveal the surface morphology of samples, which can be visualized as a macroscopical observation for the surface crystal. Sparse little particles can be seen for neat PA, ranging from hundreds of nanometers to several nanometers in size (in Fig. 7(a)). For 1 wt.% CNT/PA-SDBS (see Fig. 7(b)), the size of crystalline particles seems to be larger than neat PA, but is also very sparsely; in addition, the surface of sample is discontinuous, presenting many holes, which cannot be found in neat PA system, proving the addition of CNT would break the integrity of membrane formed through the processes comprising of spin-coating and subsequent solvent evaporation. Similar morphology can also be found in 3 wt.% CNT/PA-SDBS system (in Fig. 7(c)), but the particle size is smaller than the 1 wt.% one; the presenting particles, probably, could be ascribed to the crystalline particle of sample. The increasing particle size shows the addition of CNT will favor the growth of crystalline

Table 1 The heat of fusion ΔH fc(J/g) values of samples calculated from DSC curves

Samples	PA	PA-SDBS	0.1 wt.%CNT/ PA-SDBS
ΔH fc(J/g)	11.3	9.4	9.8
Samples	0.5 wt.%CNT/ PA-SDBS	1 wt.%CNT/ PA-SDBS	3 wt.%CNT/ PA-SDBS
ΔH fc(J/g)	11.1	9.1	9.2

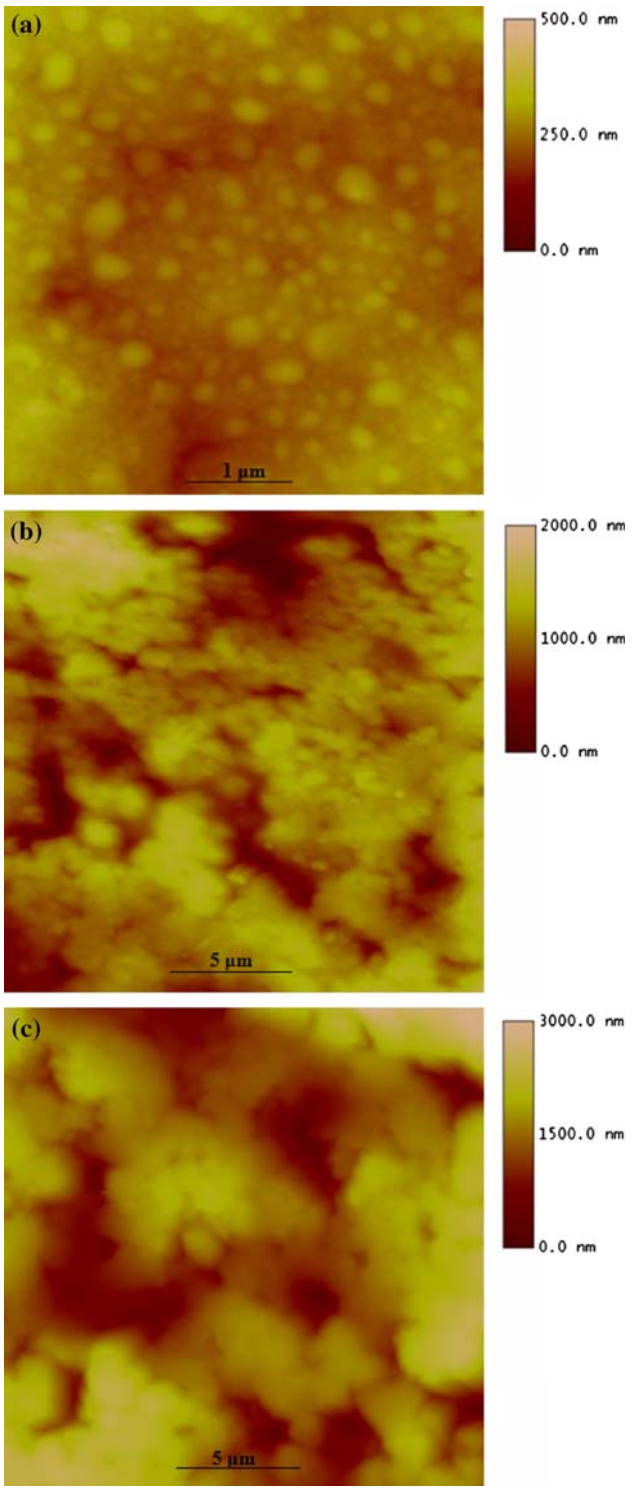

Fig. 7 AFM images of samples, (**a**): neat PA, (**b**): 1 wt.% CNT/PA-SDBS, (**c**): 3 wt.% CNT/PA-SDBS

particles. And the sparse and less perfect crystallite, moreover, implies the poor crystallization of the sample. This respect could be also evidenced from the consistent XRD and DSC results in Figs. 5 and 6, respectively.

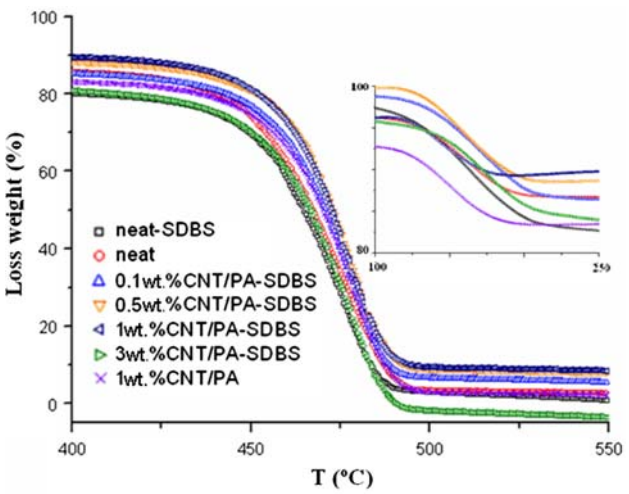

Fig. 8 TGA data (in nitrogen) for neat PA and composites

It has been shown that CNTs have extremely high thermal conductivity [26, 27]. By improving the carbon nanotube-polymer interfacial interaction it is possible to impart the excellent thermal conductivity of CNTs to the composite material, and it is known that the enhanced thermal conductivity of the composite can facilitate heat transport and thus increase its thermal stability [28, 29]. We therefore investigated the thermal properties of the composites, and their TGA profiles are given in Fig. 8. The temperature at the maximum mass loss rate in the TGA curve corresponds to the accepted thermal decomposition temperature of the composite. The results shown in Fig. 8 indicate that composites with higher MWCNT loading decompose at higher temperature, and this demonstrates that incorporation of MWCNTs increases the thermal stability of the composite. In our experiments, the thermal decomposition temperature of PA is approximately 422 °C, and this value gradually increases as more MWCNTs are incorporated into the composite until the decomposition temperature reaches a value of 435 °C at a level of 1 wt.% MWCNTs. However, when the level of MWCNT reaches 3 wt.%, the decomposition temperature is decreased reversely, almost the same TGA curves as neat PA. In addition, the incorporation of SDBS also has an impact on the thermal conductivity of composite, reducing the decomposition temperature of composite.

Mechanical properties

Dynamic mechanical analysis measurements were performed on PA matrix and carbon nanotube composites. As a semi-quantitative results to inspect the strengthen effect of CNT, Fig. 9 displays the dynamic stress-strain curves for different samples at ambient temperature, which

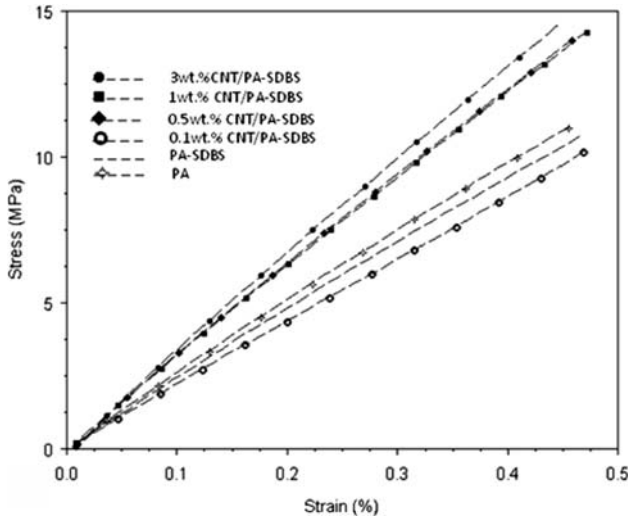

Fig. 9 The dynamic stress-strain curves for different samples at ambient temperature

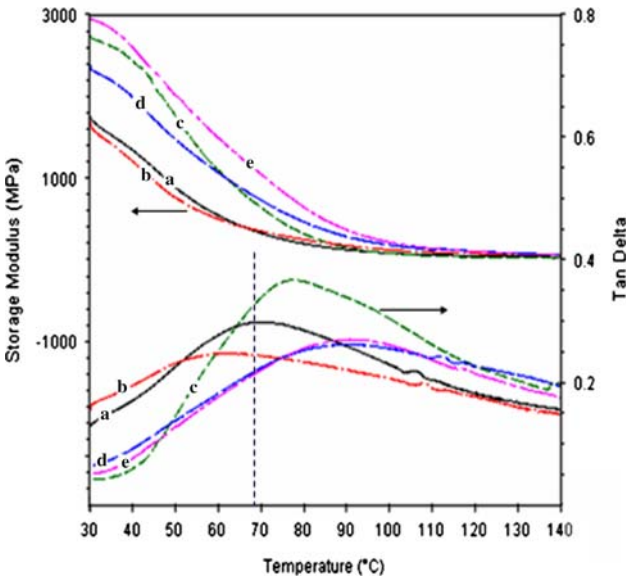

Fig. 10 The storage modulus (E') and loss factor (tanδ) versus temperature DMA curves for neat PA and its composites. MWCNT contents, (**a**): 0%, (**b**): 0.1 wt.%, (**c**): 0.5 wt.%, (**d**): 1 wt.%, (**e**): 3 wt.%

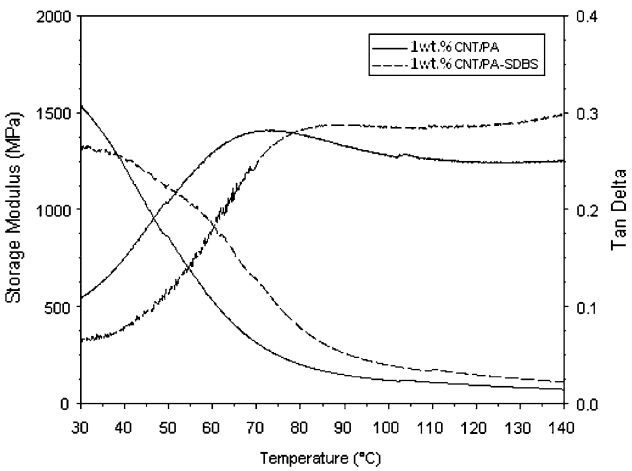

Fig. 11 The storage modulus (E') and loss factor (tanδ) versus temperature DMA curves for 1 wt.% CNT/PA without surfactant SDBS and 1 wt.% CNT/PA-SDBS composites

indicates a large increasing mechanical property obtained for the composites. This observation is more obvious when the CNT contents increase from 0.1 wt.% to 0.5 wt.%, but this trend is less evident from 0.5 wt.% to 3 wt.%, revealed only as little increasing stress. On the other hand, it can be seen that the addition of surfactant SDBS does not greatly influence the mechanical property of PA. And as unexpected, however, at the CNT content of 0.1 wt.%, the stress of composites is lower than that of neat PA and PA/SDBS systems.

To better understand the strengthening effect of CNT, especially that at high temperature, the temperature dependence of storage modulus (E') for all samples are also probed and the results are displayed in Figs. 10 and 11. At low temperature the polymer is in the glassy state and the modulus decreases with increase in temperature. When the temperature is up to ca 40 °C, a rapid decrease corresponding to the glass–rubber transition in the elastic tensile modulus is observed. This modulus drop was ascribed to an energy dissipation phenomenon involving the cooperative motions of long chain sequences [30]. The storage modulus at 90 °C and the glass transition points (normally defined as the peak temperature in tanδ curves in the DMA test) of the different samples are summarized in Table 2. For 0.1 wt.% CNT/PA-SDBS composites, a little decrease of mechanical property is found at lower temperature (<60 °C) comparing with neat PA, which is in consistent with the result of stress-strain in Fig. 8. With increasing temperature, the storage modulus of neat PA decreases more quickly than composites; so at high temperature, the composite system can still retain high mechanical property, almost one times greater than the neat one. When the CNT contents higher than 0.5 wt.%, the storage modulus of carbon nanotube filled sample is increased largely in the whole temperature range of DMA measurement and this observation is more evident especially near the melting temperature. From Table 2, it is found that at 90 °C, the storage modulus of composites containing surfactant, compared to neat PA, increases 1.2, 2.6, and 3.5 times for 0.5, 1, and 3 wt.% CNT loading, respectively (as found in Table 2). This observation verifies that the CNT could serve as an intensifier to enhance the mechanical property of PA evidently.

Combining the DMA results and above analysis of crystallization through the DSC and XRD measurement, we can conclude the increasing mechanical property for

Table 2 The storage modulus value E' (MPa) at 90 °C and tanδ peak value (°C) of samples

Samples	PA	0.1 wt.%CNT/ PA-SDBS	0.5 wt.%CNT/ PA-SDBS
E'(MPa)	76.97	146.6	169.6
T_g(°C)	69.9	60.0	75.8
Samples	1 wt.%CNT/ PA-SDBS	1 wt.%CNT/PA	3 wt.%CNT/ PA-SDBS
E'(MPa)	280.4	146.0	346.8
T_g(°C)	84.1	69.0	86.9

composites should be ascribed to the strengthening effect from the CNT component, not being caused by the variation of crystalline phase and crystallinity resulted in by the addition of CNT. Correspondingly, the elevating T_g temperature (last line in Table 2) is also a strong evidence: at 3 wt.% CNT content, the T_g temperature reach to 86.9 °C, increasing about 27 °C comparison with neat PA (69.9 °C). This effect is indeed in agreement to previous studies which showed that the constraining of polymer chains by attachment to silica or to nanotube surfaces results in an increasing of T_g [5, 31, 32].

Conversely, some investigations indicated that for the MWCNTs/PA6 blend composites, the T_g did not change with respect to PA6, due to a lower/weak covalent linkage between MWCNTs and PA6 [22, 33]. In this experiment, no any modification for MWCNTs was proceeded and the increasing T_g was probably ascribe to the strong interaction existing between MWCNTs and aromatic PA chains, which restrict the movement of PA chains and lead to the increasing T_g temperature.

In this case, in order to get a close check whether adding surfactant is help to increase the strengthening effect of CNT to neat PA, the thermal mechanical property of 1 wt.% CNT/PA-SDBS and 1 wt.% CNT/PA are comparably investigated. As exhibited in curves from Fig. 11, which clearly indicates after the surfactant was added, the storage modulus and T_g for composites are both improved, i.e., increasing about one times for storage modulus and 15 °C for T_g temperature (see Table 2). This observation also proves that the addition of surfactant is help to disperse the carbon nanotube into PA matrix, and accordingly increasing the mechanical property and T_g of composites.

Conclusion

Semi-aromatic polyamide(PA)/(MWCNT) composite was prepared through a high-speed shearing (11,000 rpm) step for 2 h in the presence of surfactant SDBS. To the analysis of morphology, crystallization and dynamical mechanical property show the presence of SDBS help to disperse the MWCNT, largely enhancing the mechanical property; the storage modulus (E') of 3 wt.% MWCNT/PA-SDBS at 90 °C is 3.5 times greater than PA and the (T_g) increases about 27 °C. Similar phenomena are not found in MWCNT/PA composite without surfactant. Simultaneously, the filled MWCNT was not the effect of crystalline phase and crystallinity of PA, proving the increasing mechanical property for these composites is the origin from the strengthening effect of MWCNT itself, not being caused by the change of crystalline phase and crystallinity resulted in by the addition of MWCNT. The increasing T_g probably ascribe to the strong interaction existing between MWCNTs itself and PA chains, restricting the movement of PA chains. Which indicate that the strong interaction exists between the carbon nanotube itself and aromatic polymer chains. Just through a simple method dispersing the carbon nanotube into aromatic polymer can obtain a large enhancing mechanical property, without complicated modification for carbon nanotube carried out, thus, the damage to carbon nanotube structure is also smaller. This result will be applied to the preparation of other aromatic polymer-CNT composites.

Acknowledgement This work was partially subsidized by Henan Innovation Project for University Prominent Research Talents ("HAIPURT") program.

References

1. Wang ZL, Poncharal P, de Heer WA (1999) First IUPAC workshop on advanced materials: nanostructured systems, Hong Kong, July 14–18
2. Wagner HD, Lourie O, Feldman Y, Tenne R (1998) Appl Phys Lett 72:188
3. Calvert PD (1999) Nature 399:210
4. Carran SA, Ajayan PM, Blau WJ, Carroll DL, Coleman JN, Dalton AB, Davey AP, Drury A, Mccarthy B, Maier S, Strevens A (1998) Adv Mater 10:1091
5. Liu L, Barber AH, Nuriel S, Wagner HD (2005) Adv Funct Mater 15:975
6. Meincke O, Kaempfer D, Weickmann H, Friedrich C, Vathauer M, Warth H (2004) Polymer 45:739
7. Chang TE, Jensen LR, Kisliuk A, Pipes RB, Pyrz R, Sokolov AP (2005) Polymer 46:439
8. Gong X, Liu J, Baskaran S, Voise RD, Young JS (2000) Chem Mater 12:1049
9. Ruan SL, Gao P, Yang XG, Yu TX (2003) Polymer 44:5643
10. Chen JZ, Qu LJ, Li XF, Jiang AJ, Niu MJ, Wang JW (2005) J Appl Polymer Sci 97:1586
11. Liu LQ, Zhang S, Hu TJ, Guo ZX, Ye C, Dai LM, Zhu DB (2002) Chem Phys Lett 359:191
12. Qin Y, Liu L, Shi J, Wu W, Zhang J, Guo Z, Li Y, Zhu D (2003) Chem Mater 15:3256
13. Dalmas F, Chazeau L, Gauthier C, Masenelli-Varlot K, Dendievel R, Cavaille JY, ForrÓ L (2005) J Polym Sci: Part B: Polym Phys 43:1186
14. Moore VC, Strano MS, Haroz EH, Hauge RH, Smalley RE, Schmidt J, Talmon Y (2003) Nano Lett 3:1379

15. Vigolo B, Penicaud A, Coulon C, Sauder C, Pailler R, Journet C, Bernier P, Poulin P (2000) Science 290:1331
16. Israelachvili JN (1992) Intermolecular and surface forces, 2nd edn. Academic Press, San Diego
17. Konyushenko EN, Stejskal J, Trchová M, Hradil J, Kovářová J, Prokeš J, Cieslar M, Hwang J-Y, Chen K-H, Sapurina I (2006) Polymer 47:5715
18. Baibarac M, Baltog I, Lefrant S, Meveller JY, Chauver G (2003) Chem Mater 15:4149
19. Ferrer-Anglada N, Kaempgen M, Skákalová V, Dettlaf-Weglikowska U, Roth S (2004) Diam Relat Mater 13:256
20. Gao C, Jin YZ, Kong H, Whitby RL, Acquah SF, Chen GY (2005) J Phys Chem B 109:11925
21. Zeng H, Gao C, Yan D (2006) Adv Funct Mater 16:812
22. Zeng H, Gao C, Wang Y, Paul CP, Kong H, Cui X, Yan D (2006) Polymer 47:113
23. Arimoto H (1964) J Polym Sci A2:2283
24. Hummel DO (1965) Pure Appl Chem 11:497
25. Frayer PD, Koening JL, Lando JB (1972) J Macromol Sci Phys B6:129
26. Benedict LX, Louie SG, Cohen ML (1996) Solid State Commun 100:177
27. Berber S, Kwon YK, Tomanek D (2000) Phys Rev Lett 84:4614
28. Huxtable ST, Cahill GG, Shenogin S, Xue L, Ozisik R, Barone P, Usrey ML, Strano MS, Siddons G, Shim M, Keblinski P (2003) Nat Mater 2:731
29. Gao J, Itkis ME, Yu A, Bekyarova E, Zhao B, Haddon RC (2005) J Am Chem Soc 127:847
30. Dufresne A, Paillet M, Putaux JL, Canet R, Carmona F, Delhaes P, Cui S (2005) J Mater Sci 37:3915. doi:10.1023/A:1019659624567
31. Savin DA, Pyun J (2002) J Polym Sci Part B: Polym Phys 40:2667
32. Yao Z, Braidy N, Botton GA, Adronov A (2003) J Am Chem Soc 125:16015
33. Liu TX, Shen L, Chow SY, Zhang WD (2004) Macromolecules 37:7214